An indication of the existence of a solar wind strahl at 10 AU

A. P. Walsh,[1,2] C. S. Arridge,[1,3] A. Masters,[4] G. R. Lewis,[1,3] A. N. Fazakerley,[1]
G. H. Jones,[1,3] C. J. Owen,[1] and A. J. Coates[1,3]

Received 25 March 2013; revised 1 May 2013; accepted 1 May 2013; published 6 June 2013.

[1] The solar wind electron distribution is observed near and within 1 AU to consist of three components: a thermal core, a suprathermal halo, and a suprathermal strahl. The former two components are isotropic, while the strahl is field aligned and flows outward along the interplanetary magnetic field. The evolution of solar wind electrons with heliocentric distance is poorly understood; although the halo is thought to be formed through pitch angle (PA) scattering of the strahl, the responsible physical process has not been conclusively identified. Measurements of solar wind electrons throughout the heliosphere are required to solve this problem. We present the first observations of the suprathermal components of the solar wind electron distribution made outside 5 AU. We find indications of a strahl component narrower than that predicted by extrapolating observations and models of electrons in the inner heliosphere, suggesting the rate of electron pitch angle scattering in the solar wind can decrease with increasing heliocentric distance. **Citation:** Walsh, A. P., C. S. Arridge, A. Masters, G. R. Lewis, A. N. Fazakerley, G. H. Jones, C. J. Owen, and A. J. Coates (2013), An indication of the existence of a solar wind strahl at 10 AU, *Geophys. Res. Lett.*, *40*, 2495–2499, doi:10.1002/grl.50529.

1. Introduction

[2] Electrons in the solar wind near and within 1 AU have been observed to be a superposition of thermal and suprathermal components [*Feldman et al.*, 1975]. The suprathermal electrons can be described as a superposition of two populations, a diffuse, near-isotropic halo [*Feldman et al.*, 1975] and a component termed the strahl which travels outward, closely aligned along the interplanetary magnetic field (IMF) direction [*Rosenbauer et al.*, 1977]. The full width of the strahl in pitch angle (PA) space has been seen to vary from a narrow field-aligned population (i.e., 5°–20°) to one that is broader (30°–40°) in PA space [*Pilipp et al.*, 1987]. More recently, a survey of Advanced Composition Explorer (ACE) data [*Anderson et al*., 2012] found the strahl width at 1 AU to vary such that no characteristic width can be determined.

[3] The characteristics of the solar wind electron distribution are expected to vary with heliocentric distance. Between ~ 0.3 and ~ 5 AU, the relative density of the strahl has been observed to decrease, while the relative density of the halo has been observed to increase with increasing heliocentric distance, suggesting that the halo is formed through PA scattering of the strahl as the electrons travel outward [*Maksimovic et al.*, 2005; *Štverák et al.*, 2009]. Indeed, the strahl has been observed to broaden in PA space with increasing distance from the Sun, consistent with this hypothesis [*Hammond et al.*, 1996]. Broadening is expected to begin at the distance at which PA scattering starts to dominate over adiabatic focusing of the field-aligned electrons as they travel into regions of weaker magnetic field [*Owens et al.*, 2008]. Recent Cluster observations appear to show this PA scattering occurring in intense bursts, localized in space or time, rather than as a continuous process [*Gurgiolo et al.*, 2012]. Resonant interaction between the strahl electrons and whistler mode waves [e.g., *Vocks et al.*, 2005] has been proposed as a potential scattering mechanism, and there is some evidence suggesting that scattering happens more often in high-β solar wind, perhaps related to the occurrence of magnetic holes [*Crooker et al.*, 2003]. However, the exact mechanism of halo formation remains unclear.

[4] In order to properly constrain the process that broadens the strahl and therefore potentially forms the halo, measurements of solar wind electrons taken throughout the heliosphere are needed. To date, observations of the suprathermal components of the solar wind electron distribution have not been made outside the orbit of Jupiter [*McComas et al.*, 1992]. Here, we use data from the Cassini spacecraft taken during its initial orbit around Saturn, i.e., at a heliocentric distance of 10 AU, and identify a suprathermal component of electrons with an enhanced phase space density (PSD) in the expected strahl direction compared to other directions. This places a lower limit on the scattering rate from the strahl to the halo and therefore the process responsible for that scattering.

2. Data Selection and Processing

[5] A 5 day section of Cassini's initial orbit around Saturn, 19–23 August 2004, near apoapsis, was selected. This section of the initial orbit has the most favorable geometry of Cassini's tour of the Kronian system for studying the pristine solar wind. The KSO (Kronian Solar Orbital; X points from Saturn to the Sun, Z is northward and normal to the plane of Saturn's orbit, and Y completes a right-handed set) XY projection of the orbit is plotted in Figure 1. The section of the orbit from which the data were used in this study is colored blue in the figure. A cartoon bow shock and a magnetopause are included in gray for context.

[1]Department of Space and Climate Physics, University College London, Mullard Space Science Laboratory, Holmbury St. Mary, UK.
[2]Now at Science and Robotic Exploration Directorate, ESA/ESTEC, Noordwijk, The Netherlands.
[3]The Centre for Planetary Sciences at UCL/Birkbeck, London, UK.
[4]Institute of Space and Astronautical Science, Japan Aerospace Exploration Agency, Sagamihara, Japan.

Corresponding author: A. P. Walsh, Science and Robotic Exploration Directorate, ESA/ESTEC, Noordwijk, Netherlands. (awalsh@rssd.esa.int)

0094-8276/13/10.1002/grl.50529

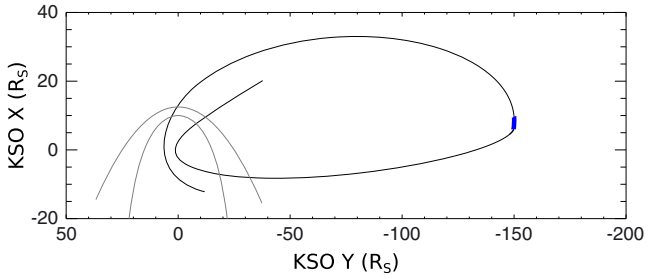

Figure 1. KSO *XY* projection of the Cassini spacecraft's initial orbit around Saturn. The 5 day section of the orbit from which the data were used in this study is highlighted in blue. A model bow shock and a magnetopause (gray) are included for reference.

[6] Electron measurements in the energy range ∼0.5–26,000 eV from the Cassini spacecraft are provided by the electron spectrometer (ELS), part of the Cassini Plasma Spectrometer (CAPS) suite [*Young et al.*, 2004]. The sensor comprises a top hat electrostatic analyzer with an instantaneous field of view (FOV) of 5° × 160° and a position-sensitive detector which is divided into eight 20° anodes. The sensor is mounted on a motorized platform, enabling it to scan roughly half the sky, giving an overall FOV of 100° × 160°. Some of the FOV of the instrument is blocked by parts of the spacecraft structure and, during the interval investigated here, the Huygens probe. These obstructions reduced the instantaneous field of view of ELS during this study to a maximum of 5° × 120°, although depending on the orientation of the magnetic field with respect to the FOV, PA coverage was not always this large. The magnetic field information used to determine the PAs of the electrons measured by ELS is provided by the Cassini magnetometer [*Dougherty et al.*, 2004].

[7] At 10 AU, the count rate of solar wind electrons with suprathermal energies is expected to be low, and individual distributions measured by ELS at those energies were dominated by noise. However, through combining and averaging individual distributions, the signal-to-noise ratio can be increased, and a mean distribution can be constructed. However, this has the disadvantage of introducing significant time aliasing into the results. A 5 day interval was chosen as a compromise between including enough data for a significant result and minimizing the amount of time aliasing. The average distribution of electrons traveling in the expected strahl direction was compared with the average distribution of electrons with a PA of 90°. In total, during the 5 day interval, ∼ 24,000 individual distributions of electrons with a PA of 90° were measured compared with ∼ 1500 individual measurements of electrons traveling in the expected strahl direction.

[8] At 10 AU, the observed Parker spiral direction is ∼ 90° from the radial direction [*Jackman et al.*, 2008] so, assuming a monodirectional strahl, electrons traveling outward along the spiral flow from ∼ $-Y$ to $+Y$ KSO. During this interval, Cassini was located dawnward of Saturn (Figure 1), so the expected strahl direction is the (anti)field-aligned direction measured while the angle between the instrument look direction and the spacecraft-Saturn line was between 90° and 270°. We thus exclude from the average distribution electrons reflected from and/or accelerated to suprathermal energies at Saturn's bow shock [e.g., *Masters et al.*, 2009]. No correction was made for either the spacecraft velocity or the solar wind bulk velocity (measurements of the latter were not routinely available during this interval), although these would be small compared to instrument energy resolution at suprathermal energies. The measurements made in the expected strahl direction were in the central anodes of the ELS detector; therefore, simultaneous measurements of electrons traveling in the expected strahl direction and those with a PA of 90° were not made.

[9] When there is a low natural flux of electrons, it is important to consider the background level and any sources of the uncertainty on the data. The ELS data have a back-

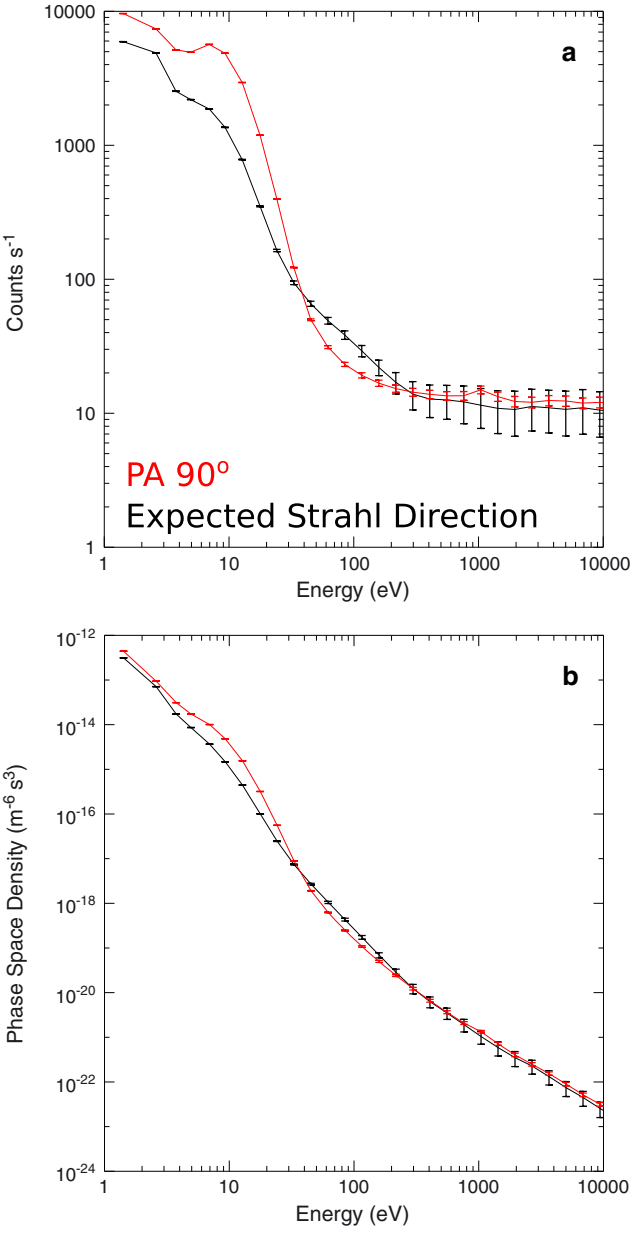

Figure 2. Mean electron distributions plotted in (a) counts s^{-1} and (b) m^{-6} s^3 (PSD) units. The black curves are electrons traveling outward along the IMF, i.e., in the expected strahl direction, while the red curves are electrons measured to have a pitch angle of 90°. Error bars show the 2σ uncertainty on the mean.

ground level of approximately 30 counts s^{-1} which is look direction dependent and time dependent and has as its source the radioisotope thermoelectric generators carried by the Cassini spacecraft [*Arridge et al.*, 2009]. This background level was subtracted from the data, and only those data points with positive count rates were included in the averages. The following sources of uncertainty were also considered: the Poisson error on the count rate, an error of 5–20% arising from data compression, and the uncertainty on the background level. These were combined using formal error propagation methods. Since the individual measurements, r_i, have different uncertainties, σ_i^2, the mean count rates, $\bar{r}$, were weighted by the uncertainties, i.e.,

$$\bar{r} = \frac{\Sigma_i \left(r_i/\sigma_i^2\right)}{\Sigma_i \left(1/\sigma_i^2\right)} \tag{1}$$

The uncertainty on the mean, $\sigma_{\bar{r}}^2$, is then given by

$$\sigma_{\bar{r}}^2 = \frac{1}{\Sigma_i \left(1/\sigma_i^2\right)} \tag{2}$$

See *Bevington and Robinson* [2003] for details.

[10] No information about the spacecraft potential was available, so no correction for this was applied to the data. However, photoelectron contamination is unlikely to affect the measured distributions at suprathermal energies.

3. Observations

[11] Average count rates as a function of energy are plotted in Figure 2a. The black curve is the count rate in the expected strahl direction, while the red curve is the count rate of electrons with a PA of 90° ± 10°. Error bars represent $2\sigma_{\bar{r}}$, calculated as described above. The associated electron distribution functions are plotted in Figure 2b with the same colors; again, error bars represent $2\sigma_{\bar{r}}$.

[12] There is a higher count rate (and hence PSD) of electrons with a PA of 90° at energies below ~ 30 eV, whereas at energies between ~ 30 eV and ~ 200 eV, there are a higher count rate and a higher PSD in the expected strahl direction (Figure 2). These differences are greater than the $2\sigma_{\bar{r}}$ uncertainties on the averages. A count rate of 10 counts s^{-1} represents ~ 1 count per accumulation and thus the effective sensitivity limit of ELS. The PA 90° curve reaches this level at ~ 100 eV and the expected strahl direction curve at ~ 300 eV.

[13] Although no simultaneous measurements of electrons traveling in the expected strahl direction and at PAs of 90° were made during the studied interval, intermediate PAs were measured at the same time as the expected strahl direction. The average electron distribution function measured in the expected strahl direction together with that at PAs separated by up to 80° from that direction is plotted in Figure 3a. For clarity, the error bars here represent the $1\sigma_{\bar{r}}$ uncertainty on the mean. The black curve is the PSD measured in the expected strahl direction (i.e., ΔPA = 0°–20°), while the colored curves show the PSD measured at PAs with an increasing angular separation (in 20° increments) from the expected strahl direction. The colored curves show an average PSD which becomes progressively closer to that measured at a PA of 90° with increasing angular separation from the expected strahl direction. This can be more clearly seen in Figure 3b, in which the PSD at various energies has been plotted as a function of ΔPA. The error bars here again represent 1σ, and the dashed colored lines show the half-maximum PSD for the relevant energy. There is indeed a systematic decrease in PSD with increasing angular separation from the expected strahl direction.

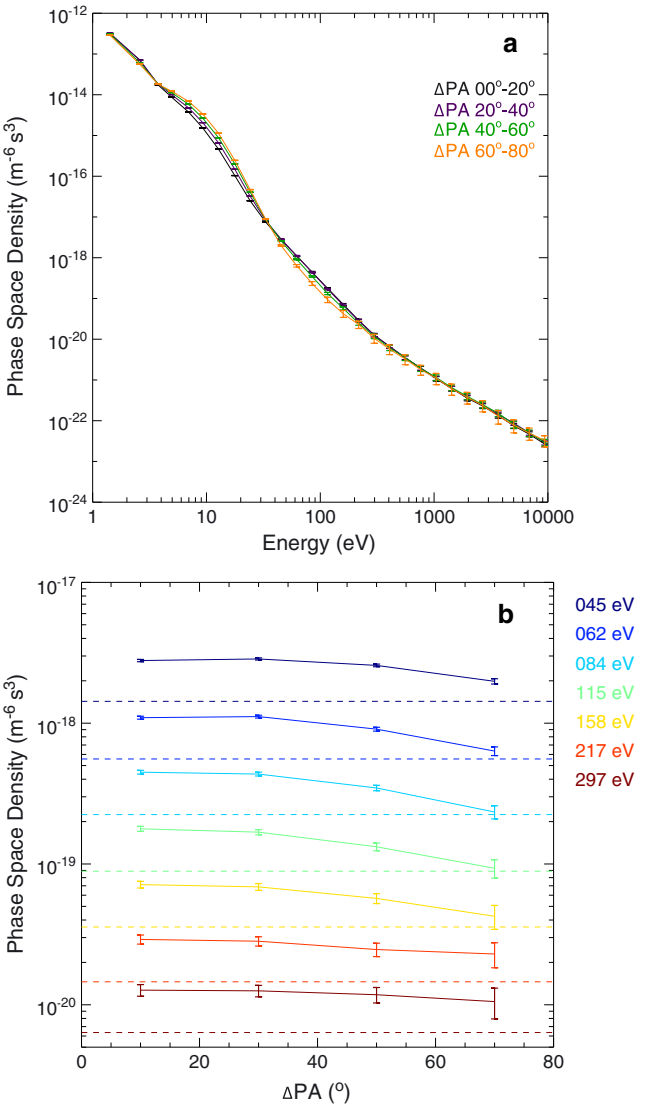

Figure 3. (a) The different colored curves represent the mean PSD of electrons organized by pitch angle relative to that of the expected strahl direction (ΔPA). Contrary to the averages plotted in Figure 2, these averages are limited to those distributions taken when the expected strahl direction was within the field of view of ELS. Here, the error bars show the 1σ uncertainty on the mean. (b) The mean PSD of suprathermal electrons is plotted as a function of pitch angle relative to that of the expected strahl direction (ΔPA). The different colored curves represent different energies of electrons. The dashed lines represent the half-maximum PSD for the equivalent energy. The error bars show the 1σ uncertainty on the mean.

4. Discussion

[14] A simple 1-D model distribution function, the sum of a Maxwellian and a kappa distribution, representing the core and halo, respectively, i.e.,

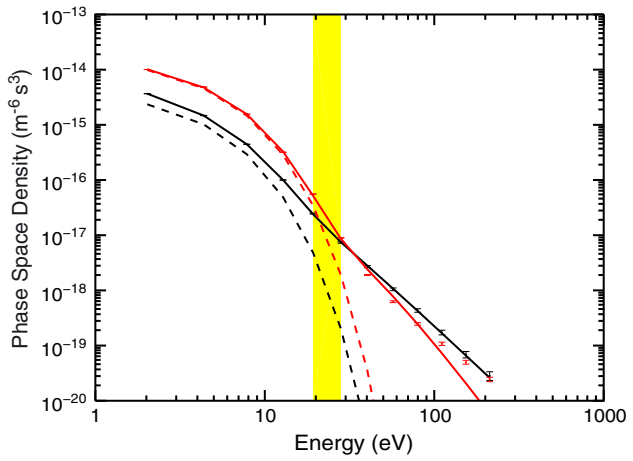

Figure 4. The solid lines are the sum of a Maxwellian (core) and a kappa (halo) distribution fit to the same data plotted in Figure 2, corrected for an estimated 6 V spacecraft potential, while the dashed lines are only the Maxwellian component. The yellow-shaded area represents the energy bins between which the PA 90° data increase to twice the Maxwellian component of the fit.

$$f(v) = n_c \left(\frac{m_e}{2\pi k_b T_c}\right)^{\frac{3}{2}} e^{-\frac{m_e v^2}{2k_b T_c}} + n_h \left(\frac{m_e}{\pi k_b T_h (2\kappa_h - 3)}\right)^{\frac{3}{2}} \cdot \frac{\Gamma(\kappa_h + 1)}{\Gamma(\kappa_h - 0.5)} \left(1 + \frac{m_e v^2}{k_b T_h (2\kappa_h - 3)}\right)^{-\kappa_h - 1} \quad (3)$$

was fit using the Levenberg-Markwardt algorithm [*Markwardt*, 2009] separately to the expected strahl direction and PA 90° averages. The n_c and n_h are the densities and T_c and T_h the temperatures of the core and halo, respectively. κ_h is the kappa index for the halo.

[15] Based on the gradient change evident between 4 V and 6 V in Figure 2, a 5 V spacecraft potential correction was applied to the average distributions before fitting. The results of the fits are plotted in Figure 4, and the fit parameters are listed in Table 1. The increasing difference between the PA 90° data and the fit at higher energies is the result of the count rate at those energies being close to the sensitivity limit of ELS. The yellow-shaded region in Figure 4 represents the energy bins between which the Maxwellian component of the fit for PA 90° fell below half the observed value. We have identified this as the energy range 19–28 eV within which the suprathermal breakpoint lies. This is lower than that typically observed closer to the Sun, although the breakpoint energy is known to decrease with increasing heliocentric distance [*McComas et al.*, 1992]. The T_c returned from the PA 90° fit was 35,400 K (i.e., $\sim$ 3 eV), so our results for the breakpoint energy are consistent with the theory [*Scudder and Olbert*, 1979] that it should be $\sim 7T_c$. The PA 90° parameters were used because the Maxwellian component does not accurately reproduce the core in the expected strahl direction. A simple model such as this is expected to overestimate n_h and underestimate n_c since the halo is not truncated at thermal energies [*Štverák et al.*, 2009]. The halo temperatures for both fits lie within the predicted range for 10 AU based on the results of *Maksimovic et al.* [2005].

[16] Given that the two distribution functions plotted in Figure 2b are averages of two sets of measurements that were not made at the same times, the difference in PSD between electrons traveling in the expected strahl direction and those with a PA of 90° could be due to temporal variation in the solar wind. By examining intermediate PAs that were measured simultaneously with the expected strahl direction (Figure 3), this possibility can, to the extent possible when considering time averages, be rejected. We thus conclude that on average, the PSD along the magnetic field direction is higher at suprathermal energies (this would also suggest that the thermal core of the solar wind had a higher PSD perpendicular to the magnetic field than in the expected strahl direction, although we do not focus on that here). This could be due to the presence of either a distinct, field-aligned strahl component or a halo with an anisotropy such that $T_{h\parallel} > T_{h\perp}$. For either scenario, the PSD at a given energy should decrease with increasing angular separation from the magnetic field (ΔPA), reaching a minimum at a PA of 90°. This expected decrease in PSD at suprathermal energy is evident in Figure 3, although without full PA coverage it is impossible to unambiguously distinguish between the two explanations. However, the results of the fitting are more consistent with the presence of a strahl: $T_{h\perp} > T_{h\parallel}$. Given the possible mixing of the core and halo components in the model, it is also useful to consider the combination of core and halo temperatures. Here, $(n_c T_c + n_h T_h)/(n_c + n_h)$ is also higher for PA 90° electrons. The higher PSD at suprathermal energies in the expected strahl direction is reproduced by a higher density and a lower κ.

[17] While they do not represent an unambiguous detection, the results presented in Figures 2–4 are consistent with the presence of a distinct strahl component to the solar wind electron distribution observed at 10 AU. The PSD of the suprathermal electrons of a given energy systematically decreases with increasing angular separation from the expected strahl direction. The net difference remains even after taking into account the 2σ error on the mean, suggesting that this result is significant. Indeed, Student's t test confirms that the suprathermal components of the mean distribution functions plotted in Figure 2b are significantly different at confidence levels in excess of 99%, although it should be noted that this, in itself, is not proof of the existence of a strahl.

[18] An estimate of the angular half width of the strahl can be made if this is defined as the width at which the PSD drops to its half maximum [*Hammond et al.*, 1996]. Within error, this occurs at a ΔPA of 60°–80° for energies of 84 eV–158 eV (Figure 3), but at other suprathermal energies, the PSD does not decrease to half maximum within the angular range sampled by ELS, suggesting that a lower limit on the angular half width of the strahl at 10 AU is 70° $\pm$ 10° during the studied interval. *Hammond et al.* [1996] suggested a linear relationship between strahl width

Table 1. Fit Parameters Rounded to Two Significant Figures

Parameter	Strahl Direction	PA 90°
n_c (cm^{-3})	0.026	0.12
n_h (cm^{-3})	0.018	0.069
T_c (K)	32,000	35,000
T_h (K)	90,000	110,000
κ	1.92	3.35

and radial distance from the Sun, based on Ulysses data taken primarily between 1 and 2.5 AU. For strahl electrons at energy of 115 eV, this relationship is given by $Width = (34 \pm 24)° + (30 \pm 14)°R_{AU}$. Extrapolating to 10 AU, this predicts a width ranging between 170° (slightly higher than our observed value) and in excess of 360°, suggesting that the wider strahls detected by Ulysses were completely scattered to form the halo by the time they reached the orbit of Saturn, and only the narrower strahls detected inside the orbit of Jupiter persist as a distinct component in the solar wind electron distribution as far as 10 AU from the Sun. Our observations are also consistent with recent work by *Anderson et al*. [2012], who found an anticorrelation between strahl width and strahl intensity. Given the relative density of the strahl is known to decrease with increasing heliocentric distance [e.g., *Maksimovic et al.*, 2005; *Štverák et al.*, 2009], a narrower than average strahl is not only more likely to remain distinct at 10 AU but also more likely to be detectable at that heliocentric distance.

[19] *Owens et al.* [2008] reproduced the radial evolution of strahl widths observed by *Hammond et al.* [1996] using a model comprising adiabatic focusing and PA scattering, the rate of which was independent of heliocentric distance. Our results therefore suggest that the rate of PA scattering does not always remain constant with heliocentric distance and can instead reduce. *Crooker et al.* [2003] found that the strahl was less likely to be detected at 1 AU in higher-β solar wind, suggesting an increased rate of scattering in high-β plasmas. Given that the plasma β in the solar wind is expected to increase with radial distance, a scattering rate that reduces with heliocentric distance suggests that enhanced scattering is not an intrinsic property of higher-β solar wind. The effectiveness of scattering by whistler waves depends on available wave power below the electron gyrofrequency, f_{ce} [*Vocks et al.*, 2005]. Given that whistler wave power decreases with heliocentric distance [*Hu et al*., 1999], as does f_{ce}, a decreasing pitch angle scattering rate from the strahl to the halo with increasing heliocentric distance is consistent with whistler waves providing the scattering mechanism.

5. Conclusion

[20] Based on data from the Cassini CAPS-ELS instrument, we have presented the first observations of the suprathermal population of solar wind electrons beyond the orbit of Jupiter, the properties of which are consistent, for the period studied, with the presence of a distinct strahl component with a half width of at least 70° at 10 AU. The existence of a strahl that far from the Sun suggests that the rate of pitch angle scattering from the strahl to the halo decreases with heliocentric distance, consistent with the scattering being produced by interactions with whistler waves. It should be noted that we cannot exclude the possibility that the data represent observations of an anisotropic halo. Furthermore, the strahl is known to be highly variable in terms of both angular width and strength [*Anderson et al.*, 2012], so caution is necessary when considering averages such as those presented here. This first result, then, does not necessarily extend to the general case. However, it does suggest that the Cassini CAPS-ELS data set is suitable as the basis for a wider investigation of the properties and evolution of solar wind electrons from 1 to 10 AU.

[21] **Acknowledgments.** A.P.W., A.N.F., C.J.O., and A.J.C. were funded by UK STFC grant ST/H00260X/1. A.P.W. now holds an ESA Fellowship. C.S.A. held a UK STFC Postdoctoral Fellowship, G.R.L. was funded by the UK Space Agency, and G.H.J. held a UK STFC Advanced Fellowship. Portions of this work were carried out at the International Space Science Institute, Berne, Switzerland. We acknowledge the Cassini instrument teams for the provision of the data used in this study.

[22] The Editor thanks Peter Gary and an anonymous reviewer for their assistance in evaluating this paper.

References

Anderson, B. R., R. M. Skoug, J. T. Steinberg, and D. J. McComas (2012), Variability of the solar wind suprathermal electron strahl, *J. Geophys. Res.*, *117*, A04107, doi:10.1029/2011JA017269.

Arridge, C. S., L. K. Gilbert, G. R. Lewis, E. C. Sittler, G. H. Jones, D. O. Kataria, A. J. Coates, and D. T. Young (2009), The effect of spacecraft radiation sources on electron moments from the Cassini CAPS electron spectrometer, *Planet. Space Sci.*, *57*, 854–869, doi:10.1016/j.pss.2009.02.011.

Bevington, P. R., and D. K. Robinson (2003), *Data Reduction and Error Analysis for the Physical Sciences*, chap. 4, pp. 56–57 (3rd edn), McGraw Hill, London.

Crooker, N. U., D. E. Larson, S. W. Kahler, S. M. Lamassa, and H. E. Spence (2003), Suprathermal electron isotropy in high-beta solar wind and its role in heat flux dropouts, *Geophys. Res. Lett.*, *30*, 1619, doi:10.1029/2003GL017036.

Dougherty, M. K., et al. (2004), The Cassini magnetic field investigation, *Space. Sci. Rev.*, *114*, 331–383, doi:10.1007/s11214-004-1432-2.

Feldman, W. C., J. R. Asbridge, S. J. Bame, M. D. Montgomery, and S. P. Gary (1975), Solar wind electrons, *J. Geophys. Res.*, *80*, 4181–4196, doi:10.1029/JA080i031p04181.

Gurgiolo, C., M. L. Goldstein, A. F. Viñas, and A. N. Fazakerley (2012), Direct observations of the formation of the solar wind halo from the strahl, *Ann. Geophys.*, *30*, 163–175, doi:10.5194/angeo-30-163-2012.

Hammond, C. M., W. C. Feldman, D. J. McComas, J. L. Phillips, and R. J. Forsyth (1996), Variation of electron-strahl width in the high-speed solar wind: Ulysses observations, *Astron. Astrophys.*, *316*, 350–354.

Hu, Y. Q., S. R. Habbal, and X. Li (1999), On the cascade process of Alfvén waves in the fast solar wind, *J. Geophys. Res.*, *104*, 24,819–24,834, doi:10.1029/1999JA900340.

Jackman, C. M., R. J. Forsyth, and M. K. Dougherty (2008), The overall configuration of the interplanetary magnetic field upstream of Saturn as revealed by Cassini observations, *J. Geophys. Res.*, *113*, A08114, doi:10.1029/2008JA013083.

Maksimovic, M., et al. (2005), Radial evolution of the electron distribution functions in the fast solar wind between 0.3 and 1.5 AU, *J. Geophys. Res. Space Phys.*, *110*, A09104, doi:10.1029/2005JA011119.

Markwardt, C. B. (2009), Non-linear least-squares fitting in IDL with MPFIT, in *Astronomical Data Analysis Software and Systems XVIII, Astronomical Society of the Pacific Conference Series,* vol. 411, edited by D. A. Bohlender, D. Durand, and P. Dowler, 251 p., Astronomical Society of the Pacific, San Francisco.

Masters, A., et al. (2009), Hot flow anomalies at Saturn's bow shock, *J. Geophys. Res.*, *114*, A08217, doi:10.1029/2009JA014112.

McComas, D. J., S. J. Bame, W. C. Feldman, J. T. Gosling, and J. L. Phillips (1992), Solar wind halo electrons from 1–4 AU, *Geophys. Res. Lett.*, *19*, 1291–1294, doi:10.1029/92GL00631.

Owens, M. J., N. U. Crooker, and N. A. Schwadron (2008), Suprathermal electron evolution in a Parker spiral magnetic field, *J. Geophys. Res.*, *113*, A11104, doi:10.1029/2008JA013294.

Pilipp, W. G., K.-H. Muehlhaeuser, H. Miggenrieder, M. D. Montgomery, H. Rosenbauer (1987), Characteristics of electron velocity distribution functions in the solar wind derived from the Helios plasma experiment, *J. Geophys. Res.*, *92*, 1075–1092, doi:10.1029/JA092iA02p01075.

Rosenbauer, H., et al. (1977), A survey on initial results of the Helios plasma experiment, *J. Geophys-Z. Geophys.*, *42*, 561–580.

Scudder, J. D., and S. Olbert (1979), A theory of local and global processes which affect solar wind electrons. I—The origin of typical 1 AU velocity distribution functions—Steady state theory, *J. Geophys. Res.*, *84*, 2755–2772, doi:10.1029/JA084iA06p02755.

Štverák, Š., M. Maksimovic, P. M. Trávníček, E. Marsch, A. N. Fazakerley, E. E. Scime (2009), Radial evolution of nonthermal electron populations in the low-latitude solar wind: Helios, Cluster, and Ulysses observations, *J. Geophys. Res. Space Phys.*, *114*, A05104, doi:10.1029/2008JA013883.

Vocks, C., C. Salem, R. P. Lin, and G. Mann (2005), Electron halo and strahl formation in the solar wind by resonant interaction with whistler waves, *Astrophys. J.*, *627*(1), 540–549, doi:10.1086/430119.

Young, D. T., et al. (2004), Cassini Plasma Spectrometer investigation, *Space Sci. Rev.*, *114*, 1–112, doi:10.1007/s11214-004-1406-4.